Soot Formation in Weakly Buoyant Acetylene-Fueled Laminar Jet Diffusion Flames Burning in Air

P. B. SUNDERLAND, Ü. Ö. KÖYLÜ, and G. M. FAETH*

Department of Aerospace Engineering, The University of Michigan, Ann Arbor, Michigan 48109-2118

The structure and soot properties of weakly buoyant, acetylene-fueled, laminar jet diffusion flames were studied experimentally for combustion in air at pressures of 0.125-0.250 atm. Properties along the axis, where soot processes are similar to behavior within nonbuoyant diffusion flames, were emphasized. The following measurements were made: soot volume fractions using laser extinction, temperatures using both thermocouples and multiline emission, soot structure using thermophoretic sampling and analysis by transmission electron microscopy, concentrations of major gas species using sampling and analysis by gas chromatography, and velocities using laser velocimetry. As distance increased along the axis of the present acetylene-fueled flames, significant soot formation began when temperatures exceeded roughly 1250 K, and ended when fuel-equivalence ratios decreased to roughly 1.7, where the concentration of acetylene became small. This behavior allowed observations of soot growth and nucleation for acetylene concentrations of 6×10^{-6}–1×10^{-3} kg-mol/m^3 and temperatures of 1000–2100 K. Over this range of conditions, soot growth rates were comparable to past observations of new soot in premixed flames, and after correction for effects of soot oxidation yielded essentially first-order growth with respect to acetylene concentrations with a negligible activation energy, and an acetylene/soot collision efficiency of 0.53%. Present measurements of soot nucleation rates also suggested first-order behavior with respect to acetylene concentrations but with an activation energy of 32 kcal/gmol and with rates that were significantly lower than earlier estimates in the literature. Nevertheless, uncertainties about effects of soot oxidation and age on soot growth, and about effects of surface area estimates and translucent objects on soot nucleation, must be resolved in order to adequately define soot formation processes in diffusion flames.

NOMENCLATURE

$[C_2H_2]$	molar concentration of acetylene
d	burner exit diameter
d_p	mean primary soot particle diameter
f	mixture fraction
f_s	soot volume fraction
Fr	burner exit Froude number, $u_o^2/(gd)$
g	acceleration of gravity
k_g	soot growth rate constant
k_n	soot nucleation rate constant
n	reaction order
n_p	number of primary particles per unit volume
$\overline{N}$	mean number of primary particles per aggregate
p	pressure
Re	burner exit Reynolds number, $u_o d/\nu_o$
S	soot surface area per unit volume
t	time
T	temperature
u	streamwise velocity
v_g	soot growth velocity
w_g	soot growth rate
w_n	soot nucleation rate
X_i	mole fraction of species i
z	streamwise distance

Greek Symbols

ν	kinematic viscosity
ρ	gas density
ρ_s	soot density

Subscripts

o	burner exit condition

INTRODUCTION

Soot processes within nonpremixed hydrocarbon-fueled flames are important because they affect the durability and performance of propulsion systems, the hazards of unwanted fires, the pollutant and particulate

emissions from combustion processes, and the potential for developing capabilities for computational combustion. Motivated by these observations, the present investigation involved an experimental study of the structure and soot properties of round laminar jet diffusion flames, seeking an improved understanding of soot formation (growth and nucleation) within diffusion flames. Present work emphasized weakly buoyant diffusion flame behavior that is typical of many practical applications [1].

Past studies of soot processes in flames have been reviewed by Haynes and Wagner [2] and Glassman [3]. A popular configuration for experimental studies of soot processes in diffusion flames has been the buoyant laminar jet diffusion flame that typically is used for measurements of laminar smoke point properties [3]. Representative recent studies of these flames include the work of Kent and Wagner and coworkers [4-10], and Dobbins and Santoro and coworkers [11-17], among others [18-23]. It is well known, however, that buoyancy affects soot processes within laminar jet diffusion flames because soot particles are too large to diffuse so that they convect at flow velocities aside from small effects of thermophoresis. This behavior causes soot particles to mainly nucleate near the flame sheet and initially move toward fuel-rich conditions within buoyant laminar diffusion flames, while they mainly nucleate near the cool core of the flame and move directly toward fuel-lean conditions within nonbuoyant laminar diffusion flames [1-3]. As a result, the soot nucleation and growth processes of buoyant and nonbuoyant laminar jet diffusion flames are quite different, providing incentive for studying soot processes for nonbuoyant flame conditions of significant practical interest. Additionally, a limitation of past studies of soot processes in diffusion flames [2-22] is that both soot properties and the local reactive environment were not sufficiently defined for detailed consideration of soot formation processes.

In contrast to studies of soot processes within laminar diffusion flames, significant progress concerning soot formation has been made from studies of fuel-rich premixed laminar flames. Representative investigations along these lines

include Bockhorn et al. [23, 24], Harris and Weiner [25-27], and Ramer et al. [28]. The findings of these studies indicated that soot mainly is produced by particle growth rather than nucleation, that the reaction between acetylene and soot particles mainly is responsible for soot growth, and that the rate of soot growth decreases with increasing residence time (age) [23-29]. Nevertheless, the relevance of these results for premixed flames to soot processes within diffusion flames has not been established.

In view of this status, the present investigation had two main objectives, as follows: (1) to complete measurements of both soot and flame properties within weakly buoyant, acetylene/air, laminar jet diffusion flames, and (2) to exploit these results to gain a better understanding of processes of soot growth and nucleation within laminar diffusion flames.

EXPERIMENTAL METHODS

Apparatus

Present measurements involved weakly buoyant, acetylene/air, laminar jet diffusion flames at low pressures, exploiting the fact that the effective buoyant acceleration scales as p^2g for laminar jet diffusion flames [30]; therefore, present tests involved pressures on the order of 0.1 atm to yield effective gravitational levels on the order of 0.01 g.

The test arrangement consisted of a round fuel jet injecting vertically upward, surrounded by a slow concentric flow of air. The flames burned along the axis of a vertical, windowed, cylindrical chamber having a diameter and length of 300 mm. The top and bottom of the chamber consisted of porous metal plates that separated the flame chamber from plenum chambers for air inflow and exhaust outflow and provided a uniform distribution of air flow over the flame chamber cross section. The fuel and air flows were measured with rotameters, calibrated in turn by wet-test meters, while the exhaust flow was removed using a vacuum pump. The flames were ignited by a hot-wire coil that could be retracted from the burner exit once ignition was complete. The entire test chamber could be traversed in the vertical and

horizontal directions in order to accommodate rigidly mounted optical instruments.

Instrumentation

Soot volume fractions were measured by deconvoluting laser extinction measurements for chord-like paths through the flames, similar to Refs. 11, 31, and 32. The data were reduced assuming that soot optical properties satisfy the small-particle (Rayleigh) scattering limit, which was justified because scattering was small. Refractive indices were taken from Dalzell and Sarofim [33], similar to past work [31, 32]. Experimental uncertainties of these measurements (95% confidence) are estimated to be less than 10% for $f_s > 0.1$ ppm.

In regions where soot was absent, gas temperatures were measured with bare wire Pt/Pt–10% Rh thermocouples having 270 μm diameter junctions. These measurements were corrected for radiation errors based on emissivities from Bradley and Entwhistle [34]. Experimental uncertainties of these measurements (95% confidence) were less than 50 K. Temperatures within soot-containing regions were found using multiline emission measurements similar to Refs. 35–37. This involved deconvoluting spectral radiation intensities for chord-like paths through the flames and finding temperatures from measurements at three line pairs: 600/750, 700/830, and 600/830 nm. Temperature differences between the average and any of the line pairs were less than 30 K while experimental uncertainties (95% confidence) of these measurements are estimated to be less than 50 K.

Soot structure was measured using thermophoretic sampling and analysis by transmission electron microscopy (TEM), similar to Refs. 14, 15, and 32. Effects of soot aggregate size cause a negligible sampling bias for $\bar{N}$ for present test conditions [32, 38]. Primary particle diameters also were very nearly monodisperse, with a standard deviation less than 10%. Experimental uncertainties (95% confidence) of these properties were dominated by finite sampling limitations, and were as follows: mean primary particle diameter, $d_p < 10\%$ and mean number of primary particles per aggregate, $\bar{N} < 20\%$. The number of primary soot particles

per unit volume, n_p, was computed from the other measurements, as follows:

$$n_p = 6f_s / \left(\pi d_p^{\,3} \right). \tag{1}$$

The resulting experimental uncertainties (95% confidence) for n_p are less than 32% for $f_s > 0.1$ ppm.

Gas compositions were measured by sampling and analysis using gas chromatography, similar to Ref. 31. A stainless-steel radiatively cooled sampling probe was used, having a port diameter of 2.1 mm. Acetylene was the only hydrocarbon present in significant quantities in the test flames; therefore, major gas species considered during gas analysis were as follows: N_2, O_2, C_2H_2, CO_2, CO, H_2O, and H_2. Experimental uncertainties of these measurements generally were less than 15% for mole fractions greater than 0.5%, dominated by uncertainties in measuring chromatogram areas.

In order to find soot processes as a function of time, streamwise velocities were measured based on laser velocimetry (LV), using aluminum oxide seeding particles, similar to Ref. 31. Experimental uncertainties (95% confidence) of the velocity measurements were less than 5%, dominated by calibration uncertainties.

Test Conditions

The four test flames are summarized in Table 1. The burner flows involved C_2H_2/N_2 mixtures with combustion in coflowing air at 0.125–0.250 atm. Visible flame lengths were 50 mm ($z/d = 15.2$), while the position of the flame tips (where the stoichiometric flame sheet reaches the axis) were in the range $z/d = 9.5$–15.2. Characteristic residence times for convection from the burner exit to the flame tip were 16.9–22.6 ms. Reynolds and Froude numbers were 80–149 and 27–256, respectively. Radiative heat loss fractions were 29%–34%.

Contamination of acetylene with acetone can be a problem for studies of acetylene reaction phenomena [39–41]. Present tests generally involved acetone mole fractions less than 2%.

<div align="center">TABLE 1</div>

<div align="center">Summary of the Test Flames[a]</div>

Test Flame	1	2	3	4
Pressure (atm)	0.250	0.188	0.125	0.250
Burner flow (% C_2H_2 by vol.)	100	100	100	59
C_2H_2 flow rate (cm^3/s)	8.12	13.6	25.0	8.96
N_2 flow rate (cm^3/s)	—	—	—	6.24
Air flow rate (cm^3/s)	395	755	1450	395
Burner exit velocity (mm/s)[b]	939	1570	2880	1760
Air coflow velocity (mm/s)[b]	5.27	10.1	19.4	5.27
Stoich. flame length (z/d)	9.5	13.9	15.2	12.2
Char. res. time (ms)	19.7	22.6	16.9	19.4
Re $(-)$[b]	80	100	122	149
Fr$(-)$[b]	27	76	256	96
Rad. heat loss (% LHV)	34.2	32.3	29.4	31.7

[a] Laminar round jet diffusion flames with 3.3 mm inside diameter burner, a visible flame length of roughly $z/d = 15.2$, and C_2H_2/N_2 mixtures flowing from the burner in an air coflow. Purified grade acetylene (99.6% purity), prepurified grade nitrogen (99.98%) purity.

[b] Nominal average value based on an injection temperature of 298 ± 2 K.

Thus, the effect of acetone contamination at this level was evaluated using the purifying train of Hamins et al. [39] to reduce the acetone concentration to 0.1%, finding negligible differences from the soot and flame properties measured at the higher acetone concentrations.

RESULTS AND DISCUSSION

Flame Structure

All the results considered in the following are for conditions along the axis of the flames, where mixture fractions decrease monotonically along a soot path similar to behavior in nonbuoyant diffusion flames. The general properties of the test flames will be illustrated using measurements for Flame 1, which involved pure acetylene at the burner exit with combustion in air at a pressure of 0.250 atm. TEM photographs of soot near the start and near the end of soot formation within Flame 1 are illustrated in Figs. 1 and 2. The present soot is seen to be typical of past observations of soot in flame environments [14, 15, 32]. Thus, at a particular location in the flame, the soot consists of roughly spherical primary soot particles having nearly constant diameters, collected into aggregates having widely varying numbers of primary particles per aggregate.

The degree of aggregation, quantified as $\overline{N}$, increases with increasing residence time.

An interesting feature of the results illustrated in Figs. 1 and 2 is that d_p is larger near the start (Fig. 1) than near the end (Fig. 2) of soot formation for the present soot path along the flame axis. This highlights an early observation of Tesner [42, 43] that the surface growth of soot persists to temperatures much lower than those required for significant soot particle nucleation (inception). This behavior causes rapid growth of the limited number of soot particles present near the start of the soot formation region, producing large primary particles, as observed in Fig. 1. Subsequently, accelerating nucleation rates create additional primary soot particles whose shorter growth period causes the average value of d_p to become smaller, as seen by comparing Figs. 1 and 2, even though overall soot concentration levels are increasing.

Another interesting feature of the TEM photographs is the presence of single (unaggregated) particles that are more translucent in appearance on the TEM photographs than the primary soot particles contained in the conventional soot aggregates. These more translucent objects were most evident near the start of soot formation (see Fig. 1) and essentially disappear in the region where most of the soot growth occurred (see Fig. 2). Notably,

Fig. 1. TEM photograph of soot aggregates along the axis of the weakly-buoyant laminar acetylene/air jet diffusion flame at 0.25 atm. (Flame 1): near the start of soot formation at $z/d = 2.9$ or a residence time of 4.2 ms. Note, TEM calibration mark is 200 nm long.

Fig. 2. TEM photograph of soot aggregates along the axis of the weakly-buoyant laminar acetylene/air jet diffusion flame at 0.25 atm. (Flame 1): near the end of the soot formation at $z/d = 5.7$ or a residence time of 10.8 ms. Note, TEM calibration mark is 200 nm long.

Megaridis and Dobbins [15] observe similar objects near the start of soot formation along the axis of buoyant ethylene/air diffusion flames at atmospheric pressure, which they suggest may be a liquid phase associated with the early stages of soot formation. Unfortunately, it was not possible to resolve the role of these translucent particles in the soot formation process during the present investigation.

Both soot and flame properties along the axis of Flame 1 are illustrated in Fig. 3. These results are plotted in terms of residence time, i.e., the elapsed time for a fluid parcel to convect from the burner exit, with the residence time to reach the flame sheet (the characteristic residence time) noted on the figure as a reference. Species concentrations illustrated in the figure, as well as corresponding results for Flames 2 and 3, are in excellent

agreement with past measurements of state relationships for major gas species as a function of mixture fraction at atmospheric pressure [31, 44]. Temperature reaches a maximum well before both the flame tip and the region of greatest soot production, which suggests significant effects of continuum radiation from soot, and possibly effects of incomplete combustion due to the presence of substantial concentrations of CO and soot, on temperatures within the flame.

Significant levels of soot formation, based on increasing values of soot volume fractions, only are observed when temperatures exceed roughly 1250 K for Flame 1 in Fig. 3, which is typical of all the present flames as well as past observations [2–4]. The end of soot formation, which roughly corresponds to conditions where the maximum value of f_s is reached because
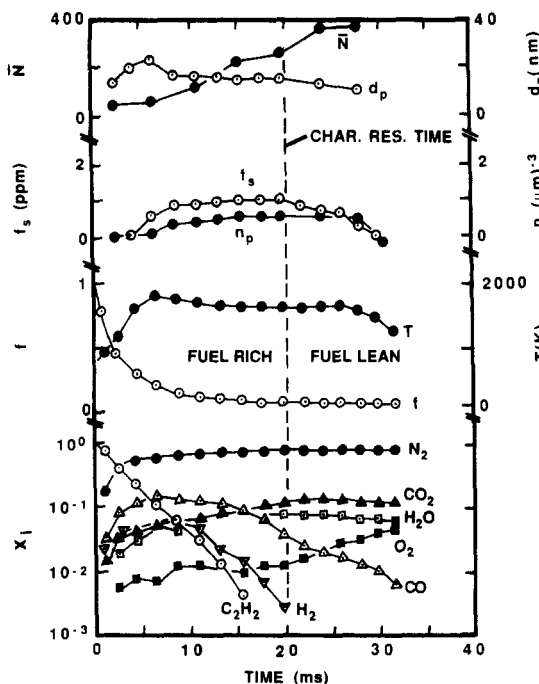
Fig. 3. Soot and flame properties along the axis of the weakly buoyant laminar acetylene/air jet diffusion flame at 0.25 atm. (Flame 1).

and nucleation in diffusion flames. As noted earlier, soot surface growth, rather than soot nucleation, dominates soot mass production. Additionally, effects of thermophoresis are small so that soot convects along streamlines because soot aggregates are too large to diffuse. Finally, the surface area available for soot growth was found by assuming that soot aggregates approximate constant diameter spherical primary particles that meet at a point. Then defining the soot growth rate, w_g, as the rate of increase of soot mass per unit soot surface area and time, conservation of soot mass along a streamline under these assumptions yields

$$w_g = \rho_s v_g = (\rho/S)d(\rho_s f_s/\rho)/dt, \qquad (2)$$

where v_g is the soot growth velocity. The soot surface area per unit volume, S, in Eq. 2 can be found from

$$S = \pi d_p^2 n_p = 6f_s/d_p, \qquad (3)$$

where the last equality of Eq. 3 follows from Eq. 1. The local density in Eq. 2 was found from present concentration and temperature measurements, assuming an ideal gas mixture of the major gas species and neglecting the volume of soot (which was only present at ppm levels). The soot density in Eq. 2 was taken to be $\rho_s = 1850$ kg/m^3, as discussed by Puri et al. [16]. Finally, the temporal derivative in Eq. 2 was found from three-point least-squares fits of the argument of the derivative, $\rho_s f_s/\rho$.

Based on existing observations, soot growth was associated with acetylene concentrations. In particular, observations of premixed flames generally correlate soot growth rates with acetylene concentrations [23–29]. Additionally, soot formation ended when acetylene disappeared and acetylene was the only hydrocarbon present in significant quantities within the present diffusion flames, as noted earlier. Thus, the following expression for w_g was studied:

$$w_g = k_g(T)[C_2H_2]^n, \qquad (4)$$

where $k_g(T)$ normally is an Arrhenius expression. Evaluation of Eq. 4 using the present measurements for various values of n, how-

gas densities are relatively uniform in this region, generally occurs when the concentration of acetylene becomes small. This condition is reached well before the flame sheet is reached, i.e., at a fuel-equivalence ratio of roughly 1.7. Notably, the end of the soot formation region occurred at similar conditions within the other three flames. As mentioned in connection with Figs. 1 and 2, the relationship between soot concentrations and primary particle diameters is complex for these flames due to interactions between soot nucleation and growth. Thus, d_p reaches a maximum well before f_s does, with the intervening region involving a large increase of n_p due to rapid nucleation. Nucleation eventually ceases, however, near the maximum f_s condition, where acetylene disappears, as noted earlier. In contrast to the complex behavior of d_p, however, the aggregation of soot particles causes a progressive increase of $\bar{N}$ with time.

Soot Growth

Present measurements along the axis of the four test flames were used to study soot growth

ever, suggested no temperature dependence for k_g. This behavior implies a small activation energy, which agrees with past suggestions of low activation energies for recombination-like soot growth processes [2, 23, 24, 29, 42, 43]. Thus, a correlation of present measurements was sought by simply plotting w_g as a function of the molar concentration of acetylene as illustrated in Fig. 4. Present test conditions yielded a range of acetylene concentrations of roughly 6×10^{-6}–1×10^{-3} kg-mol/m^3, a range of temperatures of 1250–2100 K, and a corresponding range of the observed soot growth velocities of roughly 0.01–10 μm/s. Over this range of conditions an empirical fit of the measurements was found which is illustrated in Fig. 4. Based on the units w_g (kg/m^2 s) and [C$_2$H$_2$] (kg-mol/m^3), this fit can be expressed as

$$w_g = 4560\,[\text{C}_2\text{H}_2]^{1.65}. \qquad (5)$$

The standard deviation of the power in Eq. 5 is 0.18, and the correlation coefficient of the fit is 0.89. Thus, present gross measurements of soot growth exhibit an order with respect to the concentration of acetylene (95% confidence) within the range 1.29–2.01.

The order of soot growth with respect to acetylene concentrations observed in Fig. 4 is high compared with past suggestions based on

measurements of soot growth in premixed flames [23–28]. The premixed flame data from these references has been plotted in Fig. 4 to provide a direct comparison with present diffusion flame measurements. The fuels used in the premixed flame experiments were propane, ethylene, toluene and methane, although acetylene dominated hydrocarbon concentrations in the region where soot growth measurements were made. The experiments of Bockhorn et al. [23, 24] involved a pressure of 0.15 atm while the remaining experiments were carried out at atmospheric pressure. Estimates of soot surface areas for the premixed flames were obtained from original sources, and were based on analysis of extinction and scattering measurements. Finally, rates of soot growth in premixed flames exhibit an effect of age, with the rate of growth decreasing as the residence time increases for a given ambient environment, as discussed earlier. This behavior is indicated by the vertical span of the premixed flame data in Fig. 4, with the largest w_g representing new soot at relatively small residence times (4–15 ms).

The premixed flame data illustrated in Fig. 4 are qualitatively similar to present measurements in diffusion flames. In particular, the growth rates of new soot in premixed flames approach the growth rates observed in the present diffusion flames (which have comparable residence times). However, the growth rates in the premixed flames consistently are lower than in the diffusion flames. While an effect of age could be responsible for this behavior, the apparent reduction of growth rates in premixed flames also could be caused by overestimation of the soot surface area due to use of simplified soot optical theories, with uncertainties about soot refractive indices being a contributing factor [32]. In particular, Harris and Weiner [25, 26] find that direct B.E.T. soot surface area measurements (see Brunauer et al. [45] for a description of this technique) were roughly a factor of two lower than the optical measurements, which is sufficient to explain the discrepancy between their new soot growth data and the present measurements. Additionally, the acetylene concentration ranges of the individual premixed flame studies are rather narrow to provide an accurate de-
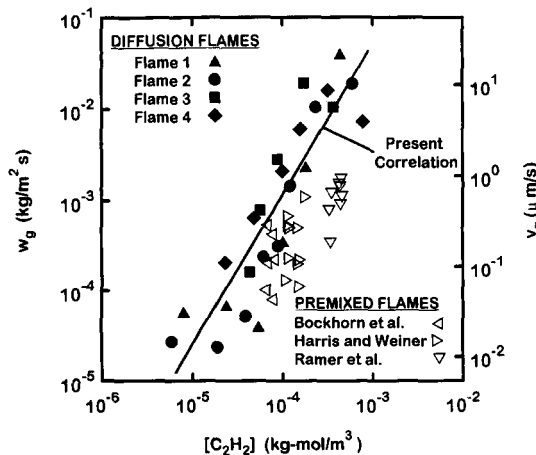

Fig. 4. Correlation of present gross soot growth rates along the axis of the weakly buoyant laminar acetylene/air jet diffusion flames, as well as measured soot growth rates within premixed flames from Refs. [23–28].

termination of the reaction order with respect to acetylene concentration, while complications due to effects of aging prevent merging the various premixed flame results to find the reaction order with respect to acetylene.

A concern about present measurements of soot growth in diffusion flames is that effects of soot oxidation could mask the actual growth behavior found from the measurements illustrated in Fig. 4, particularly when acetylene concentrations become small near the end of the soot growth region. This possibility prompted consideration of soot oxidation by O_2, CO_2, H_2O, and OH using present measurements of species concentrations and temperatures along the axis. Reaction of soot with H_2O was small in the soot growth region, based on the rate expressions found in Johnstone et al. [46]. Similarly, OH concentrations should remain small as long as fuel gases are present [49, 50], which implies that the OH soot oxidation mechanism of Neoh et al. [51] can be ignored in the soot growth region as well. Conversely, soot oxidation by O_2, and to a lesser degree by CO_2, were determined to be significant in the soot growth region. In particular, the presence of oxygen mole fractions of roughly 0.01 in the soot growth region, see Fig. 3 and the generalized state relationships of Ref. 37, imply significant potential for direct reaction between oxygen and soot. Based on the recent discussion of soot oxidation by Puri et al. [17], the direct oxidation of soot in the soot growth region was estimated using the rate expression of Nagle and Strickland-Constable [52], which was confirmed later by Park and Appleton [53]. Additionally, the presence of CO_2 mole fractions up to 0.07 in the soot growth region provides some potential for reaction between CO_2 and soot; this mechanism was treated using the approach described in Libby and Blake [47] but the corresponding corrections of w_g were relatively small. In order to check the combined O_2, H_2O, and CO_2 soot oxidation mechanisms, the predictions were compared to present measurements of soot oxidation rates in the fuel-lean portions of the four test flames; on average, predictions exceeded measurements by a factor of roughly 7 : 1. Based on this observation, present estimates of soot oxidation rates probably are

somewhat overestimated; this effect will be dealt with subsequently.

The present soot growth rates, corrected for soot oxidation in the soot growth region, are plotted as a function of acetylene concentration in Fig. 5. The correction for soot oxidation only becomes significant near the end of the soot growth region when observed growth rates become small. The net effect of the correction is to yield the following best fit correlation, based on the same units as Eq. 5, which is shown on the plot:

$$w_g = 11.0 \, [C_2H_2]^{0.90}. \tag{6}$$

The standard deviation of the power in Eq. 6 is 0.10, and the correlation coefficient of the fit is 0.87. Thus, the correlated data exhibit an order with respect to acetylene (95% confidence) within the range 0.70–1.10, which is not statistically different from unity. In addition, growth rate displayed no statistically significant variation with temperature, implying a negligible activation energy. Prompted by these observations, the corrected data were used to estimate a collision efficiency for acetylene, which is defined as the ratio of the corrected growth rate to the growth rate that would result if each C_2H_2/soot-surface collision added a soot mass of 24 kg/kgmol, finding a collision efficiency of 0.53% with an uncertainty (95% confidence) of 0.15% over the present test range.
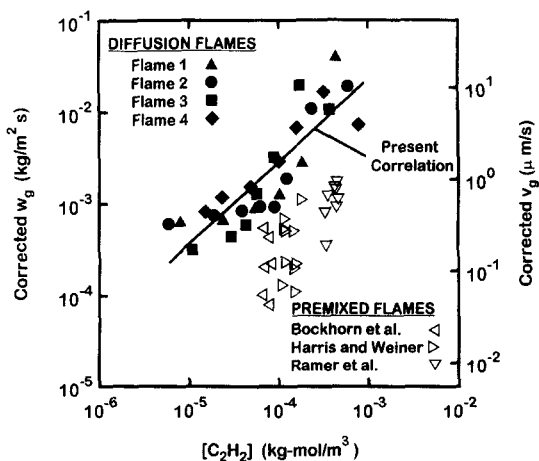

Fig. 5. Correlation of present net soot growth rates along the axis of the weakly buoyant laminar acetylene/air jet diffusion flames, after correction for soot oxidation, as well as measured soot growth rates within premixed flames from Refs. 23–28.

It also was determined that the corrections for oxidation had only a small impact on present estimates of soot growth collision efficiency; for example, eliminating measurements where the oxidation corrections exceeded 50% of the observed growth rate, yielded a collision efficiency of 0.61%, which is not statistically different from the earlier estimate. Furthermore, this entire process was repeated using the results of Bradley et al. [54] for carbon oxidation by CO_2 and H_2O, along with the results of Nagle and Strickland-Constable [52] for carbon oxidation by O_2, yielding a soot growth collision efficiency of 0.58%, which also is not statistically different from the earlier result. Additionally, in contrast to existing premixed flame measurements, also plotted on Fig. 5, where age causes soot growth collision efficiencies to progressively decrease [23–28], no effect of age was observed for present measurements of collision efficiencies in diffusion flames (for a residence time range of 3–15 ms). Finally, the oxidation corrections cause an increase in the differences between the growth rates in the present diffusion flames and new soot in premixed flames (cf., Fig. 4), however, these differences still are comparable to effects of uncertainties in optical estimates of soot surface areas for premixed flames, discussed earlier. Nevertheless, uncertainties about estimates of soot oxidation rates in diffusion flame environments [17], as well as potential effects of soot age on growth rates in both premixed [23–28] and diffusion flame environments, clearly merit further study in order to better define the soot growth process.

Soot Nucleation

Present measurements along the axis of the four test flames also were used to study the mechanism of soot nucleation. The soot nucleation rate, w_n, was defined as the rate of increase of the number of primary particles per unit volume and time. Based on the same assumptions used to determine soot growth rates from Eq. 2, the expression for soot nucleation rates for motion along a streamline becomes:

$$w_n = \rho d(n_p/\rho)/dt. \qquad (7)$$

The soot nucleation rates were correlated in terms of acetylene concentrations, similar to the earlier considerations of soot growth, i.e.,

$$w_n = k_n(T)[C_2H_2]^n, \qquad (8)$$

where $k_n(T)$ is an Arrhenius expression. Equation 7 was evaluated based on the present measurements; finding ρ and determining the argument of the derivative while locally smoothing the data using three-point least squares fits, in the same manner as for soot growth. The measurements indicated that first-order behavior for nucleation was reasonable, in agreement with earlier assessments of soot nucleation for various soot formation processes [2, 42, 43, 55].

Present soot nucleation measurements are plotted as a function of temperature, assuming first-order kinetics, in Fig. 6. The range of the present data is as follows: acetylene concentrations of 6×10^{-6}–1×10^{-3} kg-mol/m^3, temperatures of 1000–2100 K and k_n of 10^{-6}–10^{-2} s^{-1}. The scatter of the soot nucleation data is appreciable due to the strong sensitivity of n_p to d_p through Eq. 1. Based on the units w_n (kg-mol/m^3 s), $[C_2H_2]$ (kg-mol/m^3) and T(K),
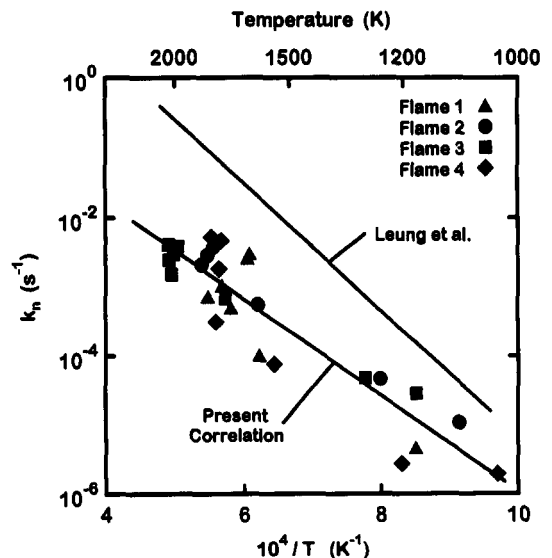

Fig. 6. Correlation of present soot nucleation rates along the axis of the weakly buoyant laminar acetylene/air jet diffusion flames, as well as earlier results for soot nucleation rates due to Leung et al. [55].

the present measurements yield the following first-order nucleation rate correlation:

$$w_n = 10.6[C_2H_2]\exp(-16100/T), \qquad (9)$$

with a standard deviation of the activation temperature of 1340 K, an activation temperature range (95% confidence) of 13300–18800 K and a correlation coefficient of the fit of 0.92. The activation energy corresponding to the activation temperature of Eq. 9 is modest, 32 kcal/gmol, which is not particularly surprising for a recombination-like process such as soot nucleation [2, 42, 43, 55].

Leung et al. [55] recently have evaluated soot nucleation data based on optical measurements from various sources and suggest, using the same units as Eq. 9:

$$w_n = 10000[C_2H_2]\exp(-21100/T), \qquad (10)$$

which implies an activation energy of 42 kcal/gmol. Equation 10 also is plotted in Fig. 6 where it yields estimates of w_n that are roughly an order of magnitude larger than the present measurements. Discrepancies of this magnitude are not surprising, however, in view of the past uncertainties of interpreting optical measurements to find primary particle sizes needed to evaluate Eq. 9 (discussed in connection with the soot growth measurements for premixed flames). In particular, overestimation of soot surface area by the optical methods, mentioned by Harris and Weiner [25, 26], would naturally lead to overestimation of soot nucleation rates seen for the correlation of Leung et al. [55] in Fig. 6. Clearly, additional measurements are needed to better establish soot nucleation properties in diffusion flames, as well as the role of the translucent objects in the nucleation process.

CONCLUSIONS

Flame structure and soot processes were studied in weakly buoyant, acetylene/air, laminar jet diffusion flames at 0.125–0.250 atm, emphasizing processes along the axis where soot first nucleates near the cool core of the flow and experiences a monotonic decrease of mix-ture fraction along a soot path line, similar to behavior in nonbuoyant flames [1]. The major conclusions of the study are as follows:

1. Significant soot nucleation and growth began when temperatures reached roughly 1250 K, and ended when acetylene disappeared at a fuel-equivalence ratio of roughly 1.7. Maximum primary soot particle diameters along the flame axes were observed near the beginning of soot formation due to the combined effects of soot nucleation and growth.

2. Present soot growth measurements, corrected for effects of soot oxidation, yielded first-order behavior with respect to acetylene with a collision efficiency of 0.53%. Present soot growth measurements in diffusion flames exhibited negligible effects of soot age with rates somewhat larger (roughly a factor of two) than past observations of new soot in premixed flames due to Bockhorn et al. [23, 24], Harris and Weiner [25–27], and Ramer et al. [28]. However, uncertainties concerning soot oxidation rates in diffusion flames and effects of soot age, in both diffusion and premixed flames, must be resolved in order to better define soot growth processes.

3. Soot nucleation was roughly first-order with respect to acetylene concentration, with a modest activation energy of roughly 32 kcal/gmol; however, these nucleation rates were roughly an order of magnitude smaller, with a smaller activation energy, than an expression proposed by Leung et al. [55] based on earlier results in the literature. It is suspected that the approximations used by Leung et al. [55] to estimate soot surface area from optical measurements are responsible for the discrepancies but the issue merits further study.

with M. B. Colket, III, R. A. Dobbins, H. B. Palmer, R. J. Santoro and K. Seshadri.

REFERENCES

1. Sunderland, P. B., Mortazavi, S., Faeth, G. M., and Urban, D. L., *Combust. Flame* 96:97–103 (1994).
2. Haynes, B. S., and Wagner, H. Gg., *Prog. Ener. Combust. Sci.* 7:229–273 (1981).
3. Glassman, I., *Twenty-Second Symposium (International) on Combustion*, The Combustion Institute, Pittsburgh, 1988, pp. 295–311.
4. Kent, J. H., Jander, H., and Wagner, H. Gg., *Eighteenth Symposium (International) on Combustion*, The Combustion Institute, Pittsburgh, 1980, pp. 1117–1126.
5. Kent, J. H., and Wagner, H. Gg., *Combust. Flame* 47:53–65 (1982).
6. Kent, J. H., and Wagner, H. Gg., *Combust. Sci. Technol.* 41:245–269 (1984).
7. Kent, J. H., and Honnery, D. R., *Combust. Flame* 79:287–298 (1990).
8. Honnery, D. R., and Kent, J. H., *Combust. Flame* 82:426–434 (1990).
9. Kent, J. H., and Honnery, D. R., *Combust. Sci. Technol.* 75:167–177 (1991).
10. Honnery, D. R., Tappe, M., and Kent, J. H., *Combust. Sci. Technol.* 83:305–321 (1992).
11. Santoro, R. J., Semerjian, H. G., and Dobbins, R. A., *Combust. Flame* 51:203–218 (1983).
12. Santoro, R. J., and Semerjian, H. G., *Twentieth Symposium (International) on Combustion*, The Combustion Institute, Pittsburgh, 1984, pp. 997–1006.
13. Santoro, R. J., Yeh, T. T., Horvath, J. J., and Semerjian, H. G., *Combust. Sci. Technol.* 53:89–115 (1987).
14. Megaridis, C. M., and Dobbins, R. A., *Twenty-Second Symposium (Interntional) on Combustion*, The Combustion Institute, Pittsburgh, 1988, pp. 353–362.
15. Megaridis, C. M., and Dobbins, R. A., *Combust. Sci. Technol.* 66:1–16 (1989).
16. Puri, R., Richardson, T. F., Santoro, R. J., and Dobbins, R. A., *Combust. Flame* 92:320–333 (1993).
17. Puri, R., Santoro, R. J., and Smyth, K. C., *Combust. Flame*, 97:125–144 (1994).
18. Flower, W. L., and Bowman, C. T., *Combust. Sci. Technol.* 37:93–97 (1984).
19. Flower, W. L., and Bowman, C. T., *Twenty-First Symposium (International) on Combustion*, The Combustion Institute, Pittsburgh, 1986, pp. 1115–1124.
20. Garo, A., Lahaye, J., and Prado, G., *Twenty-First Symposium (International) on Combustion*, The Combustion Institute, Pittsburgh, 1986, pp. 1023–1031.
21. Garo, A., Prado, G., and Lahaye, J., *Combust. Flame* 79:226–233 (1990).
22. Saito, K., Gordon, A. S., Williams, F. A., and Stickle, W. F., *Combust. Sci. Technol.* 80:103–119 (1991).
23. Bockhorn, H., Fetting, F., Wannemacher, G., and Wenz, H. W., *Nineteenth Symposium (International)*

on Combustion, The Combustion Institute, Pittsburgh, 1982, pp. 1413–1420.
24. Bockhorn, H., Fetting, F., Heddrich, A., and Wannemacher, G., *Twentieth Symposium (International) on Combustion*, The Combustion Institute, Pittsburgh, 1984, pp. 979–988.
25. Harris, S. J., and Weiner, A. M., *Combust. Sci. Technol.* 31:155–167 (1983).
26. Harris, S. J., and Weiner, A. M., *Combust. Sci. Technol.* 32:267–275 (1983).
27. Harris, S. J., and Weiner, A. M., *Combust. Sci. Technol.* 38:75–87 (1984).
28. Ramer, E. R., Merklin, J. F., Sorensen, C. M., and Taylor, T. W., *Combust. Sci. Technol.* 48:241–255 (1986).
29. Tesner, P. A., *Combust. Flame* 85:279–281 (1991).
30. Law, C. K., and Faeth, G. M., *Prog. Energy Combust. Sci.* 20:65–113 (1994).
31. Gore, J. P., and Faeth, G. M., *J. Heat Transf.* 110:173–181 (1988).
32. Köylü, Ü. Ö., and Faeth, G. M., *J. Heat Transf.*, in press.
33. Dalzell, W. H., and Sarofim, A. F., *J. Heat Transf.* 91:100–104 (1969).
34. Bradley, D., and Entwhistle, A. C., *Br. J. Appl. Phys.* 12:708–711 (1961).
35. Cashdollar, K. L., *Appl. Opt.* 18:2595–2597 (1979).
36. Klingenberg, G., *Opt. Eng.* 24:692–696 (1985).
37. Sivathanu, Y. R., and Faeth, G. M., *Combust. Flame* 81:150–165 (1990).
38. Rosner, D. E., Mackowski, D. W., and Garcia-Ybarra, P., *Combust. Sci. Technol.* 80:87–101 (1991).
39. Hamins, A., Gordon, A. S., Saito, K., and Seshadri, K., *Combust. Sci. Technol.* 45:309–410 (1986).
40. Colket, M. B., III, Seery, D. J., and Palmer, H. B., *Combust. Flame* 75:343–366 (1989).
41. Colket, M. B., III, Seery, D. J., and Palmer, H. B., *Combust. Flame* 84:434–437 (1991).
42. Tesner, P. A., *Seventh Symposium (International) on Combustion*. The Combustion Institute, Pittsburgh, 1958, pp. 546–553.
43. Tesner, P. A., *Eighth Symposium (International) on Combustion*. The Combustion Institute, Pittsburgh, 1960, pp. 627–633.
44. Sivathanu, Y. R., and Faeth, G. M., *Combust. Flame* 82:211–230 (1990).
45. Brunauer, S., Emmett, P. H., and Teller, E., *J. Am. Chem. Soc.* 60:309–314 (1938).
46. Johnstone, J. F., Chen, C. Y., and Scott, D. S., *Ind. Eng. Chem.* 44:1564–1569 (1952).
47. Libby, P. A., and Blake, T. R., *Combust. Flame* 36:139–169 (1979).
48. Libby, P. A., and Blake, T. R., *Combust. Flame* 41:123–147 (1981).
49. Miller, J. H., Honnery, D. R., and Kent, J. H., *Twenty-Fourth Symposium (International) on Combustion*. The Combustion Institute, Pittsburgh, 1992, pp. 1031–1039.
50. Smyth, K. C., Miller, J. H., Dorfman, R. C., Mallard,

W. G., and Santoro, R. J., *Combust. Flame* 62:157–181 (1985).

51. Neoh, K. G., Howard, J. B., and Sarofim, A. F., *Particulate Carbon* (D. C. Siegla and B. W. Smith, Ed.), Plenum, New York, 1980, pp. 261–277.
52. Nagle, J., and Strickland-Constable, R. F., *Proc. Fifth Carbon Conf.* 1:154–164 (1962).
53. Park, C., and Appleton, J. P., *Combust. Flame* 20:369–379 (1973).
54. Bradley, D., Dixon-Lewis, G., El-Din Habik, S., and Mushi, E. M. J., *Twentieth Symposium (International) on Combustion*, The Combustion Institute, Pittsburgh, 1984, pp. 931–940.
55. Leung, K. M., Lindstedt, R. P., and Jones, W. P., *Combust. Flame* 87:289–305 (1991).

Comments

C. Megaridis, University of Illinois at Chicago, USA. The declining character of soot primary particle diameter (d_p) in the region of increasing soot volume fraction (f_s) was attributed to sustained soot inception along the flame axis. Was this hypothesis corroborated by your TEM observations, i.e., were soot precursor particles detected on the micrographs in these flame locations?

Authors' Reply. What was seen on the TEM photographs is typified by the examples provided in Figs. 1 and 2 of soot near the start and end of soot formation within Flame 1, respectively. In both cases, the roughly spherical primary soot particles have nearly constant diameters, and we did not observe significant numbers of smaller primary soot particles (ranging down to the smallest detectable size) that would be directly suggestive of the presence of newly formed soot particles. Thus, the conclusion concerning sustained soot nucleation (inception) follows from the observation of increasing numbers of primary soot particles per unit volume, n_p, along the axes of the flames, similar to the behavior illustrated in Fig. 3.

The reasons why large numbers of small primary soot particles were not observed in regions where soot nucleation rates were large must still be established; two possible explanations involve the rapid coagulation of small precursor soot particles, and the rapid net soot growth velocity of the soot formation region of acetylene/air diffusion flames (up to 20 nm/ms, see Figs. 4 and 5). In addition, the significance of the round translucent objects, mainly observed near the onset of soot nucleation, must still be resolved.

K. C. Smyth, NIST, USA. Comment. The question of whether or not soot particle reactivity decreases with time will be difficult to answer if nucleation persists along the flame centerline—as the authors suggest. The high reactivity of newly formed particles could mask the decreasing reactivity of the older particles.

Question. Have you compared your surface growth rates with earlier measurements in diffusion flames? Examples include Refs. 1–8.

Authors' Reply. Present data (see Fig. 3) shows quite clearly that n_p increases throughout the soot formation region for soot paths along the flame axis; thus, the presence of continued nucleation throughout the soot formation region for these paths seems reasonably demonstrated. Dr. Smyth offers an interesting hypothesis about why variations of soot particle reactivity might be difficult to resolve for soot paths along the axis of laminar jet diffusion flames as a result; clearly, this is an issue that merits study in order to better understand soot nucleation and growth in diffusion flames.

The studies cited by Dr. Smyth involve a variety of fuels, ambient pressures, soot paths and flame geometries, none of which are identical to the conditions of the present study; therefore, direct comparison of net soot growth rates may not be very illuminating. Nevertheless, the range of soot growth rates observed during the present study, 0.02–39 gm/m²s, generally bounds the ranges observed in the other studies, e.g., in the same units and assuming a constant soot density of 1850 kg/m³, 0.2–4.6 [1], 0.1–7.4 [2], 0.05–5.7 [3], 0.07–3.7 [4], 0–23 [5], 0.09–5.6 [6], 0.3–1.1 [7] and 0.03–0.9 [8].

Aside from different flame conditions, several other caveats should be noted about the comparison between present soot growth rates and those of Refs. 1–8. First of all, even though soot oxidizing species were present in the soot formation regions of all the flames, only the present results have been corrected for effects of soot oxidation. Second, the other studies did not use the complete governing equation for soot growth rate (see the present Eq. 2); in particular, Refs. 1–6 used $w_g = (\rho_s/S)df_s/dt$ (which involves the assumption that $\rho =$ constant) and Refs. 7 and 8 used $w_g = (\rho_s/2)dd_p/dt$ (which involves the assumption that $n_p/\rho =$ constant) while present flame structure measurements indicate that neither of these assumptions is justified for present test conditions and raises questions about their use in other circumstances. Additionally, soot particle sizes and surface areas were found using laser scattering, while assuming Rayleigh scattering from spherical soot aggregates, in Refs. 1–6, which is a questionable practice compared to sampling and TEM measurements used in the present study (see Ref. 32 of the paper). Finally, none of Refs. 1–8 made species concentration measurements which are

imperative for determining soot growth species, reaction order and the collision efficiency (if appropriate) of soot growth, the activation energy of soot growth, and possible effects of soot age on soot growth; thus, the absence of such data, combined with different test conditions, precludes any absolute comparisons between the present measurements and those of Refs. 1–8.

REFERENCES

1. Vandsburger, U., Kennedy, I. M. and Glassman, I., *Combust. Sci. Tech.* 39:263–285 (1984).
2. Vandsburger, U., Kennedy, I. M. and Glassman, I., *Twentieth Symposium (International) on Combustion*, 1984, pp. 1105–1112.
3. Hura, H. S. and Glassman, I., *Combust. Sci. Technol.* 53:1–21 (1987).
4. Hura, H. S. and Glassman, I., *Twenty-Second Symposium (International) on Combustion*, 1988, pp. 371–378.
5. Flower, W. L. and Bowman, C. T., *Combust. Sci. Technol.* 53:217–224 (1987).
6. Axelbaum, R. L., Flower, W. L. and Law, C. K., *Combust. Sci. Technol.* 61:51–73 (1988).
7. Megaridis, C. M. and Dobbins, R. A., *Twenty-Second Symposium (International) on Combustion*, 1988, pp. 353–362.
8. Megaridis, C. M. and Dobbins, R. A., *Combust. Sci. Tech.* 66:1–16 (1989).